

# Quasiparticle self-consistent $GW$ calculation of $\text{Sr}_2\text{RuO}_4$ and $\text{SrRuO}_3$

Siheon Ryee,<sup>1</sup> Seung Woo Jang,<sup>1</sup> Hiori Kino,<sup>2</sup> Takao Kotani,<sup>3</sup> and Myung Joon Han<sup>1,4,\*</sup>

<sup>1</sup>*Department of Physics, Korea Advanced Institute of Science and Technology (KAIST), Daejeon 305-701, Korea*

<sup>2</sup>*National Institute for Materials Science, Sengen 1-2-1, Tsukuba, Ibaraki 305-0047, Japan*

<sup>3</sup>*Department of Applied Mathematics and Physics, Tottori University, Tottori 680-8552, Japan*

<sup>4</sup>*KAIST Institute for the NanoCentury, Korea Advanced Institute of Science and Technology, Daejeon 305-701, Korea*

(Dated: April 5, 2024)

Using quasiparticle self-consistent  $GW$  calculations, we re-examined the electronic structure of  $\text{Sr}_2\text{RuO}_4$  and  $\text{SrRuO}_3$ . Our calculations show that the correlation effects beyond the conventional LDA (local density approximation) and GGA (generalized gradient approximation) are reasonably well captured by QSGW self-energy without any *ad hoc* parameter or any ambiguity related to the double-counting and the downfolding issues. While the spectral weight transfer to the lower and upper Hubbard band is not observed, the noticeable bandwidth reduction and effective mass enhancement are obtained. Important features in the electronic structures that have been debated over the last decades such as the photoemission spectra at around  $-3$  eV in  $\text{Sr}_2\text{RuO}_4$  and the half-metallicity for  $\text{SrRuO}_3$  are discussed in the light of our QSGW results and in comparison with the previous studies. The promising aspects of QSGW are highlighted as the first-principles calculation method to describe the moderately correlated  $4d$  transition metal oxides along with its limitations.

PACS numbers: 71.20.Be, 71.15.-m, 71.18.+y

## I. INTRODUCTION

Since the seminal discovery of unconventional superconductivity at  $\leq 1$  K,  $\text{Sr}_2\text{RuO}_4$  (SRO214) has been studied extensively [1]. The crystal structure of SRO214 is of  $\text{K}_2\text{NiF}_4$ -type at low temperature as shown in Fig. 1 and its normal phase is a paramagnetic metal. Its intriguing electronic behavior and superconductivity are still a subject of active study [2–9].  $\text{SrRuO}_3$  (SRO113) is a ferromagnetic metal with a transition temperature of  $T_c \sim 160$  K. The observed magnetic moment is  $\mu = 1.1$ – $1.7 \mu_B/\text{f.u.}$  [10–14] and the stable structure at low temperature is an orthorhombic perovskite with a  $\text{GdFeO}_3$ -type distortion. The electronic structure of SRO113 is located near to the half-metallicity as reported by density functional theory (DFT) +  $U$  calculations [15–17]. The thin film SRO113 is of particular interest as a widely-used bottom electrode [18–20] and is intensively studied for the possibility of a new field-effect device [21–23].

Considering their fundamental and technological importance, it is essential to understand correctly the electronic structures of SRO214 and SRO113. For SRO214, the early electronic structure calculations [24–29] showed that the states near the Fermi level ( $E_F$ ) consist of anti-bonding combinations of Ru- $t_{2g}$  and O- $2p$ , and the Fermi surface is composed of the  $\Gamma$ -centered electron-like sheets (called as  $\beta$  and  $\gamma$ ) and the X-point-centered hole-like sheet (called as  $\alpha$ ) [24–29]. The LDA (local density approximation) Fermi surface topology was in good agreement with that of de Haas-van Alphen (dHvA) experiments [30, 34], but does not seem to be with the angle-resolved photoemission spectroscopy (ARPES) [35, 36] in

the sense that one electron-like ( $\beta$ ) and two hole-like ( $\alpha$  and  $\gamma$ ) Fermi surface were observed by ARPES [35, 36]. It however turns out to be a surface effect [37–39] later. Therefore the overall features of the electronic structure can be regarded as being described well by the conventional electronic structure calculation techniques such as LDA and GGA (generalized gradient approximation).

However the details of the electronic structure are still not clearly understood. A series of recent studies that identify SRO214 as a ‘Hund’s metal’ [2–4] can be one example showing that the previous understanding based on the conventional electronic structure calculations was not enough. Also, there was a debate regarding the detailed feature of electronic levels at  $\sim -3$  eV revealed by X-ray photoemission spectroscopy (XPS) [40–43, 47, 48]. According to XPS and resonant XPS, the indication of lower Hubbard band (LHB) of Ru- $4d$  states is observed while the LDA calculation predicts that those features should be attributed mainly to the oxygen states [47]. The experimental effective mass ( $m^*/m_{\text{LDA}} \simeq 2$ – $5$ ) is also significantly larger than the LDA value [30–33]. While DMFT can be a reasonable alternative in this situation [2, 43–46], its parameter dependency has caused the discrepancy even among the DMFT results. For example, the calculations by Pchelkina *et al.* [45] and by Liebsch *et al.* [46] seem to give different answers to the nature of the states at  $\sim -3$  eV most likely due to their different choices of  $U$  and  $J$  values. Beside the ambiguity in the double-counting term in DFT+DMFT, this parameter dependency is a well known problem for the first-principles description of the correlated electron systems. It is also noted that another well-established technique, DFT+ $U$ , is not useful for paramagnetic SRO214 because of its Hartree-Fock nature which always prefers the magnetic solution [49].

For SRO113 the situation is similar with SRO214;

\*Electronic address: mj.han@kaist.ac.kr

while the overall features can be described by the conventional methods, the details are not clearly understood. Note that DFT+ $U$  can be used for this case as the ground state of SRO113 is (ferro) magnetic. For the bulk phase, LDA, LDA+ $U$ , and self-interaction correction (SIC) give the correct ferromagnetic solution although the calculated moment shows some deviations [17, 50–52]. For the thin film SRO113, however, the experimentally observed metal-to-insulator transition (MIT) and the ferromagnetic-to-nonmagnetic transition as a function of layer thickness are not consistently reproduced by these techniques [16, 53–57]. For example, the single-layer SRO113 is predicted to be either ferromagnetic or nonmagnetic depending on the choice of the exchange-correlation functional and the  $U$  values [53, 55–57]. As in the case of SRO214, DMFT has made important contributions for SRO113 [3, 4, 58, 59], but it is still not completely satisfactory because of the limitations such as the parameter dependency. Also, the details of the spectroscopic data of SRO113 needs further clarifications [60–64].

In this paper, we re-investigate the electronic structure of these two classical  $4d$  transition-metal oxide systems by using quasiparticle self-consistent  $GW$  (QSGW) [65–67] method. To the best of our knowledge, this well-established calculation technique has never been applied to the ruthenates while  $GW$  self-energy can be expected to give a good description for the metallic and weakly correlated systems. Despite of its limitation to take the Hubbard-like on-site Coulomb interactions into account, QSGW has a distinctive advantage as a fully self-consistent ‘parameter-free’ technique. Due to the recent experimental progress in making ‘complex oxide’ structures such as thin film and heterointerface, the parameter-free description of correlated systems has become more imperative. In this context, QSGW study of these classical  $4d$  systems can be of significant importance, and its ability and limitation should be carefully investigated.

Our calculations show that the effect of electronic correlations beyond LDA and GGA is reasonably well captured by QSGW procedure, and the noticeable bandwidth reduction is observed. For the paramagnetic SRO214, the effect of  $GW$  self-energy is clearly distinctive from the other many-body calculation (*e.g.*, DMFT) in that the spectral weight transfer and the LHB feature do not appear in the QSGW result. For the ferromagnetic SRO113, QSGW band structure is quite similar with the results of DFT+ $U$  and the half-metallic band structure is reproduced.

## II. COMPUTATION METHOD

### A. Quasiparticle self-consistent $GW$ method

In QSGW, the self-energy  $\Sigma(\mathbf{r}, \mathbf{r}', \omega)$  is calculated within the  $GW$  approximation, and  $H_0$  (the noninteract-

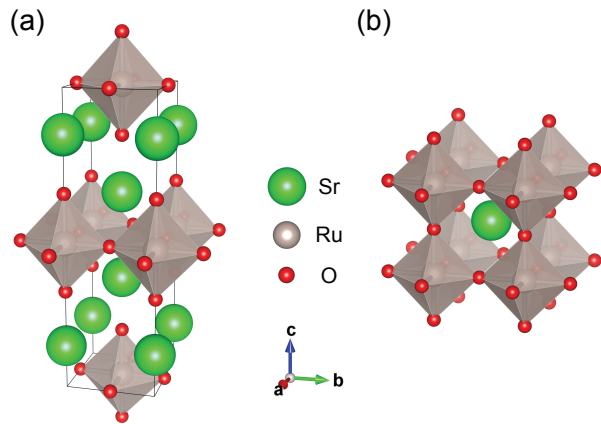


FIG. 1: The crystal structure of (a) SRO214 and (b) SRO113. The green, gray (octahedra), and red spheres represent Sr, Ru (RuO<sub>6</sub> cage), and O atoms, respectively.

ing Hamiltonian describing quasiparticles or band structures) and  $W$  (dynamically-screened Coulomb interactions between quasiparticles within random phase approximation (RPA)) is updated self consistently [65–68]. The static nonlocal one-particle exchange-correlation potential  $V^{\text{xc}}(\mathbf{r}, \mathbf{r}')$  is generated from  $\Sigma(\mathbf{r}, \mathbf{r}', \omega)$  as

$$\begin{aligned} V^{\text{xc}} &= \frac{1}{2} \int_{-\infty}^{\infty} d\omega \text{Re}[\Sigma(\omega)] \delta(\omega - H^0) + c.c. \\ &= \sum_{ij} |\psi_i\rangle \langle \psi_i| \frac{\text{Re}[\Sigma(\varepsilon_i) + \Sigma(\varepsilon_j)]}{2} |\psi_j\rangle \langle \psi_j| \end{aligned}$$

where  $\varepsilon_i$  and  $|\psi_i\rangle$  refer to the eigenvalues and eigenfunctions of  $H_0$ , respectively, and  $\text{Re}[\Sigma(\varepsilon)]$  is the Hermitian part of the self-energy [65, 66]. With this  $V^{\text{xc}}$ , one can solve a new static one-body Hamiltonian  $H_0$ , and continue to apply  $GW$  approximation until self-consistency is achieved. The distinctive feature of QSGW compared with DFT+ $U$  and DMFT is that it does not require any *ad hoc* parameters. Previous studies, ranging from atoms [69], semiconductors [66, 67, 70, 71] to the various  $3d$  transition metal oxides [66, 67, 72–74] and  $4f$  electron systems [75] have demonstrated its capacity to investigate many different types of correlated materials.

### B. Computation details

Our implementation of QSGW in ‘ecalj’ code [76] is based on the ‘augmented plane wave (APW) + muffin-tin orbital (MTO)’ method, designated by ‘PMT’ [77]. The accuracy of this scheme was proven to be satisfactory [77]. A key feature of this scheme for QSGW is that the expansion of  $V^{\text{xc}}$  can be made with MTOs, not APWs, which enables us to make the real space representation of  $V^{\text{xc}}$  at any  $\mathbf{k}$  point. In contrast to the previous approach based on FP-LMTO (full potential linearized muffin-tin

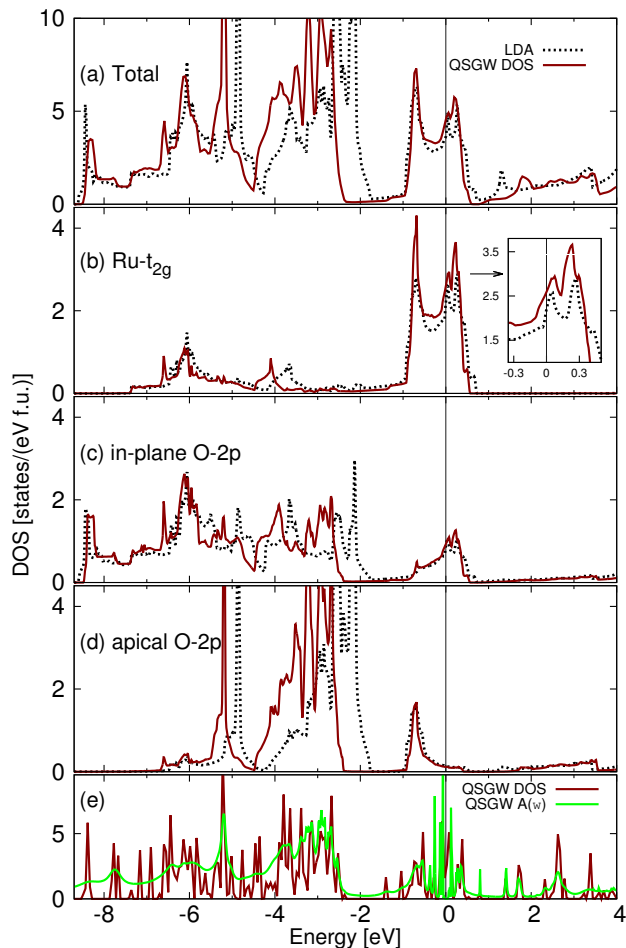


FIG. 2: The calculated (a) total DOS and (b–d) PDOS for SRO214 by LDA (black dotted lines) and QSGW (red solid lines). The spectral function  $A(\omega)$  calculated by QSGW self-energy is plotted in (e) (green solid line) along with the non-interpolated total DOS (red solid line). The Fermi level is set to zero.

orbital) [67], our scheme is free from the fine tuning of MTO parameters.

We used the in-plane and out-of-plane lattice constant of 3.87 Å and 12.73 Å, respectively, for the body-centered tetragonal SRO214. For SRO113, the cubic perovskite structure is considered as shown in Fig. 1(b). The pseudocubic lattice constant of the orthorhombic structure is 3.93 Å [78]. We used  $6 \times 6 \times 6$  [79] and  $8 \times 8 \times 8$   $\mathbf{k}$  points for the self-energy calculation in the first Brillouin zone of SRO214 and SRO113, respectively. For cubic SRO113 we also performed DFT+ $U$  calculations using OpenMX code [80] to make a comparison with previous studies. Both LDA [81] and GGA [82] functionals were used in combination with Dudarev form of DFT+ $U$  [83, 84].  $16 \times 16 \times 16$   $\mathbf{k}$  points were adopted for DFT+ $U$  calculations.

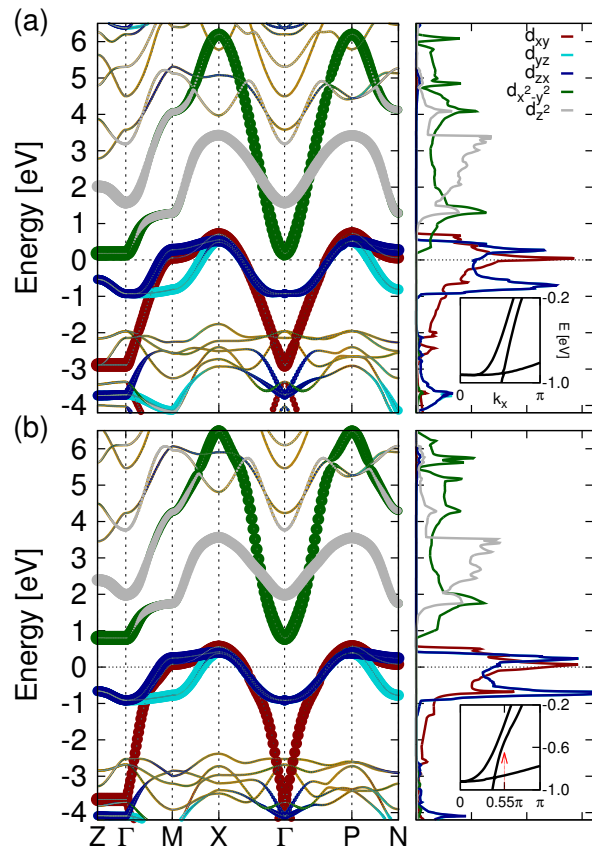


FIG. 3: The calculated band dispersion and the Ru- $d$  PDOS for SRO214 by (a) LDA and (b) QSGW. The red, cyan, blue, green and gray lines refer to the Ru  $d_{xy}$ ,  $d_{yz}$ ,  $d_{xz}$ ,  $d_{x^2-y^2}$  and  $d_{z^2}$  states, respectively. The yellow lines represent the O and Sr states (not shown in DOS). The thickness of the bands corresponds to the amount of the corresponding orbital character. The red and blue arrows represent the bandwidth of each band. The Fermi level is set to zero. The insets highlight the band dispersion at around  $-0.6$  eV along  $\Gamma$  to M ( $\pi, 0, 0$ ) by (a) LDA and (b) QSGW. A sudden change of its slope at  $(0.55\pi, 0, 0)$  is observed only in QSGW (red arrow). This feature is reflected in PDOS (see Fig. 4(b)).

### III. RESULT AND DISCUSSION

#### A. Electronic structure of $\text{Sr}_2\text{RuO}_4$

Our LDA result is in good agreement with the previous calculations [24–29], see Fig. 2 (black dotted lines) and Fig. 3. The van Hove singularity (vHS) is located at  $\sim 60$  meV above the  $E_F$  and the density of states (DOS) at  $E_F$  is  $N(E_F) \simeq 3.34$  states/(eV f.u.). The Ru- $t_{2g}$  state is dominant near  $E_F$  and is hybridized with O-2 $p$ . From Fig. 2(a), (c), and (d), one can see that the total DOS in the range of  $-4 - -2$  eV is largely attributed to the apical O-2 $p$ . The calculated band dispersion is presented in Fig. 3(a). The bandwidth of the 2D-like  $d_{xy}$  state is about two times larger than that of  $d_{yz, zx}$  states. The

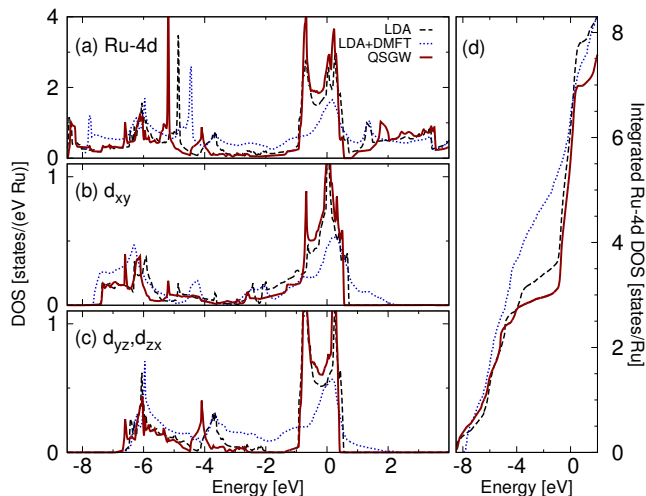


FIG. 4: (a-c) The PDOS for SRO214 calculated by LDA (black dashed lines), LDA+DMFT [45] (blue dotted lines) and QSGW (red solid lines). The  $e_g$  states in the previous LDA and DMFT study were identical [45] and are not shown here. (d) The integrated  $d$  DOS defined as  $N(E) = \int_{-\infty}^E n(\varepsilon)d\varepsilon$ , where  $n(\varepsilon)$  is the DOS at energy  $\varepsilon$ . Each value was normalized to have an equal number of states at  $E = \infty$ .  $E_F$  is set to zero.

nonbonding O-2p state is located in  $-4 - -2$  eV as can also be seen in Fig. 2(d).

The QSGW DOS is presented in Fig. 2 (red solid lines) [86]. While the overall shape of the DOS is not much different from the LDA results, some differences are observed. The two vHS located at  $\sim +60$  and  $\sim +260$  meV in LDA [24–29] become closer in QSGW shifting to  $\sim +70$  and  $\sim +220$  meV, respectively (inset in Fig. 2(b)). Both the bonding (at  $\sim -6$  eV) and the antibonding (around the  $E_F$ ) part of Ru-4d states becomes flatter in their dispersion compared to the LDA result. The  $t_{2g}$  bandwidth is slightly reduced (see Fig. 2 and 3). An interesting feature is found in the  $d_{xy}$  band dispersion along  $\Gamma$  to M. The different dispersion at  $\sim -0.6$  eV (see Fig. 3 insets) is related to the more pronounced peak in the QSGW PDOS (Fig. 4(b)). The O-2p states are shifted to the lower energy regions in QSGW (Fig. 2(c)-(d)). The Sr-4d state is further pushed up to  $\sim 4$  eV (not shown).

The further details of Ru- $t_{2g}$  state is of particular interest as the LHB feature at around  $-3$  eV has been a subject of debate [40, 43, 45–48]. Fig. 4 compares the calculated PDOS by LDA, LDA+DMFT, and QSGW. Note that the states in the range of  $-4 - -1$  eV is noticeably larger in LDA+DMFT than LDA and QSGW especially for  $d_{yz,zx}$ . It is related to the spectral weight transfer from the near- $E_F$  regions to the LHB. This is one of the main features of DMFT calculations and was the main point of the previous debate between LDA, DMFT [45, 47, 48] and the XPS experiment [40], while The QSGW result in this region is similar with the LDA

rather than the DMFT. Namely, QSGW procedure does not capture the dynamic ‘Mott-Hubbard physics’ well as in DMFT while it still takes some correlation effect into account as reflected in the bandwidth reduction and the mass enhancement. This can also be seen in Fig. 5(a). One can notice the shoulder-like LHB feature in XPS spectrum at  $\sim -3$  eV being consistent with LDA+DMFT, while both LDA and QSGW give the less states in this energy region. The theoretical spectra in Fig. 5(a) were broadened as in Ref. [45]. Not surprisingly, this LHB feature of DMFT is more pronounced in  $d_{yz,zx}$  states than in  $d_{xy}$  because of the narrower bandwidth. This point is highlighted in the integrated DOS (Fig. 4(d)). While the total number of Ru states (the integrated value up to  $E_F$ ) is basically the same in all three calculations, the DMFT value gets increased in a wider energy range. On the other hand, LDA and QSGW values are much more rapidly increased in the narrower energy range of  $-0.5 \leq \varepsilon \leq 0$  eV. Since the QSGW bandwidth is narrower than LDA, this increase is more pronounced in QSGW. Our result demonstrates the characteristic feature of QSGW to take into account of electron correlations distinctive from DMFT especially regarding the incoherent states at  $-3$  eV.

The Ru- $e_g$  bands are also affected by QSGW self-energy (see Fig. 3). The slight up-shift of the  $e_g$  antibonding bands is consistent with the previous study of SrVO<sub>3</sub> [87]. As a result, the  $d_{x^2-y^2}$  band does not touch the  $E_F$  even at  $\Gamma$  and  $Z$  point (see Fig. 3). The O-2p nonbonding state is located at  $-3.5 - -2.5$  eV in QSGW (Fig. 3), which is in better agreement with the recent ARPES result [88] than LDA.

The overall shape of the calculated Fermi surface by QSGW (see Fig. 6) is consistent with the LDA [24–29], dHvA [30, 34] and ARPES [37–39]. The inclusion of spin-orbit coupling as a perturbative correction within QSGW induces relatively small modifications at the band crossing points (not shown) [85]. The calculated effective mass at each  $\mathbf{k}$  direction is shown in Fig. 6 with color plot where  $m^*/m_{LDA}$  is estimated simply by taking the derivative of band dispersions. Along the  $\Gamma$  to X ( $\pi, \pi, 0$ ) line, the mass enhancement by QSGW is about 15% ( $m_{xy}^*/m_{LDA} \simeq 1.15$ ) for  $d_{xy}$  and 22% ( $m_{yz,zx}^*/m_{LDA} \simeq 1.22$ ) for  $d_{yz,zx}$ , respectively. For the  $\Gamma$  to M ( $\pi, 0, 0$ ) line,  $m_{xy}^*/m_{LDA} \simeq 0.83$  and  $m_{yz,zx}^*/m_{LDA} \simeq 0.78$ .

It is instructive to compare the QSGW result with the DMFT calculations and experiments while the DMFT effective mass strongly depends on the  $U$  and  $J$  values. The value reported by Mravlje *et al.* with  $U = 1.7$  and  $J = 0.0 - 0.1$  eV is  $m^*/m_{LDA} \simeq 1.7$  for both  $d_{xy}$  and  $d_{yz,zx}$  [2]. This value is significantly smaller than the other DMFT calculations, *e.g.*, by Pchelkina *et al.*,  $m^*/m_{LDA} \simeq 2.6$  and  $2.3$  for  $d_{xy}$  and  $d_{yz,zx}$ , respectively (with  $U = 3.1$  and  $J = 0.7$  eV obtained from constrained LDA) [45], and by the same group but with  $U = 2.3$  and  $J = 0.2$  eV,  $m^*/m_{LDA}$  is  $\simeq 2.3$  and  $2.0$  for  $d_{xy}$  and  $d_{yz,zx}$ , respectively [2]. These DMFT values were calculated from  $m_{DMFT}/m_{LDA} \equiv Z_{DMFT}^{-1} =$

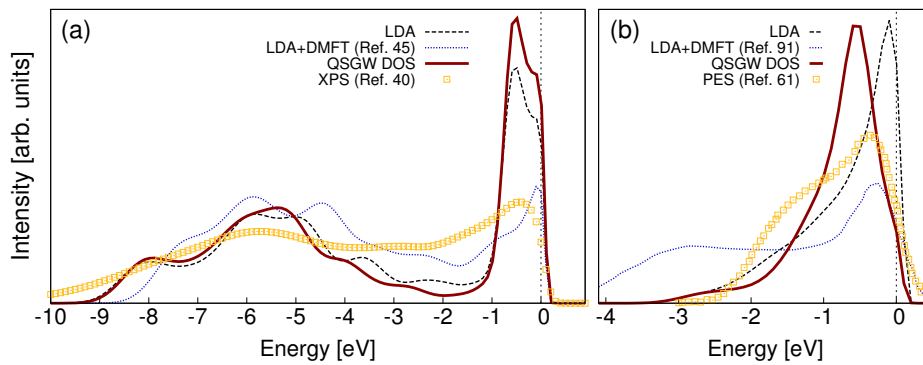


FIG. 5: The experimental and calculated spectra of (a) SRO214 and (b) Ru-4d states of SRO113. In (a), XPS spectrum (yellow dots) by Yokoya *et al.* [40] are plotted along with Gaussian-broadened DOS by LDA (black dashed line), LDA+DMFT (blue dotted line) [45], and QSGW (red solid line). In (b), PES spectrum (yellow dots) by Takizawa *et al.* [64] obtained from orthorhombic SRO113 at room temperature are plotted with Gaussian-broadened DOS of cubic SRO113 (LDA and QSGW) and orthorhombic SRO113 (LDA+DMFT [91]). Only Ru-4d states are plotted in (b). The intensities were normalized in the area under curves.

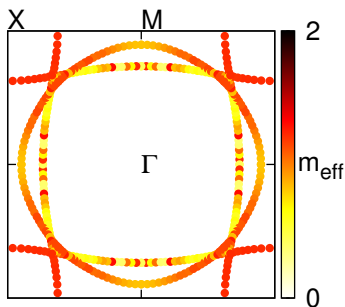


FIG. 6: The Fermi surface of SRO214 at  $k_z = 0$  plane. The color represents the calculated effective mass defined as  $m_{\text{QSGW}}/m_{\text{LDA}}$ .

$[1 - \partial_\omega \text{Re}\Sigma_{\text{DMFT}}(\omega)]_{\omega=0}$ . Our estimation from QSGW self-energy yields  $Z_{\text{QSGW}}^{-1} \simeq 1.82$  for  $d_{xy}$  and 1.71 for  $d_{yz,zx}$  [89] which is not much different from the DMFT values of 1.7 calculated by Mravlje *et al.* with  $U = 1.7$  and  $J = 0.0 - 0.1$  eV [2]. Note that  $U = 2.3$  and  $J = 0.4$  eV were suggested to be reasonable [2] in comparison to dHvA measurements [30, 32], and that the experimental values are larger than the QSGW. The early ARPES reports  $m^*/m_{\text{LDA}} \simeq 2.5$  [31] and the more recent measurement by Iwasawa *et al.* is  $m_{xy}^*/m_{\text{LDA}} \simeq 3.7$  and  $m_{yz,zx}^*/m_{\text{LDA}} \simeq 2.0$  [88]. There are two reports from the dHvA experiment;  $m_{xy}^*/m_{\text{LDA}} \simeq 4.1$  and  $m_{yz,zx}^*/m_{\text{LDA}} \simeq 3.3$  by Mackenzie *et al.* [30], and  $m_{xy}^*/m_{\text{LDA}} \simeq 5.5$  and  $m_{yz,zx}^*/m_{\text{LDA}} \simeq 3.4$  by Bergemann *et al.* [32].

## B. Electronic structure of cubic SrRuO<sub>3</sub>

The LDA result for cubic SRO113 is in good agreement with the previous studies [17, 50–52] (see Fig. 7

and Fig. 8). The calculated magnetic moment of  $\mu = 1.28\mu_{\text{B}}/\text{f.u.}$  also reasonably well agrees with the literature values of  $\mu = 1.09\mu_{\text{B}}/\text{f.u.}$  (calculated by VASP) and  $\mu = 1.26\mu_{\text{B}}/\text{f.u.}$  (calculated by SIESTA) [17]. The Sr-4d state is located above  $\sim 4$  eV (not shown) and the non-bonding state of O-2p is in  $-4 - -2$  eV. The antibonding Ru- $t_{2g}$  character dominates the near- $E_F$  region and the bonding complex is located at  $-8 - -4$  eV. A clear splitting between the up and down spin DOS is noticed and is responsible for the ferromagnetism in this material. The effect of orthorhombic distortion (not taken into account in our calculation) has been investigated previously. For example, Rondinelli *et al.* [17] showed that the result from orthorhombic structure is similar to the cubic case other than the slightly reduced exchange splitting at  $\Gamma$  point and bandwidth reduction by  $\sim 0.35$  eV for  $t_{2g}$ , 1.5 eV for  $e_g$ , and 0.6 eV for O 2p.

Several distinctive features are found in the QSGW results. First, the notable bandwidth reduction is observed (see Fig. 7 and Fig. 8). The majority spin bandwidth is reduced by  $\sim 0.7$  eV (from  $\sim 3.2$  eV (LDA) to  $\sim 2.5$  eV (QSGW)) and the minority spin bandwidth is by  $\sim 0.6$  eV (from  $\sim 3.2$  eV (LDA) to  $\sim 2.6$  eV (QSGW)). The exchange splitting is enhanced to be  $\sim 1.2$  eV which is significantly larger than the LDA value of  $\sim 0.5$  eV. We found the naive comparison of the effective mass for LDA and QSGW based on the  $\mathbf{k}$ -derivative can be misleading in SRO113 due to the different Fermi wave vectors caused by the enhanced exchange splitting in QSGW. The calculated  $Z_{\text{QSGW}}^{-1}$  for the up and down spin is 1.33 and 1.68, respectively. The effective mass of  $m_{\text{QSGW}}/m_{\text{LDA}} = 1.26$  estimated from the bandwidth ratio is reasonably well compared with some of DMFT results while the DMFT values show significant deviations ranging from 1.1 to 4.5 [59, 91–93]. The specific heat measurements report the mass enhancement of  $m^*/m_{\text{LDA}} = 3.7$  [50] and 4.5 [61]. The discrepancy reflects not only the limitation of RPA-

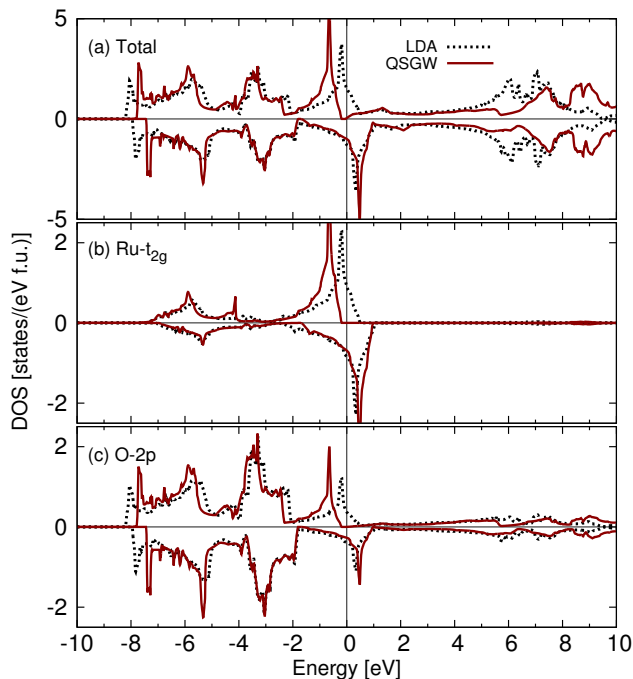


FIG. 7: The calculated (a) total DOS and (b-c) PDOS of cubic SRO113 by LDA (black dotted lines) and QSGW (red solid lines). The Fermi level is set to zero. The positive and negative DOS represent the up- and down-spin parts, respectively.

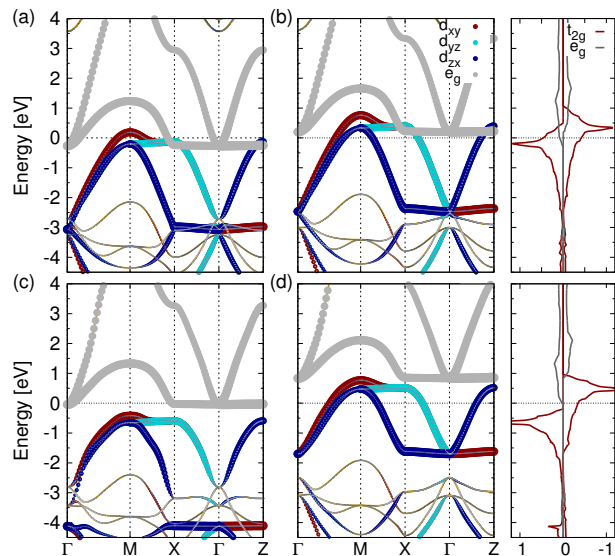


FIG. 8: The calculated band dispersion and the Ru  $d$ -orbital PDOS for cubic SRO113 by (a) LDA majority spin band, (b) LDA minority spin band, (c) QSGW majority spin band, and (d) QSGW minority spin band. The red, cyan, blue, and gray lines refer the Ru  $d_{xy}$ ,  $d_{yz}$ ,  $d_{zx}$ , and  $e_g$  states, respectively. The yellow lines represent the O and Sr states (not shown in DOS). The thickness of the bands corresponds to the amount of the corresponding orbital character. The Fermi level is set to zero.

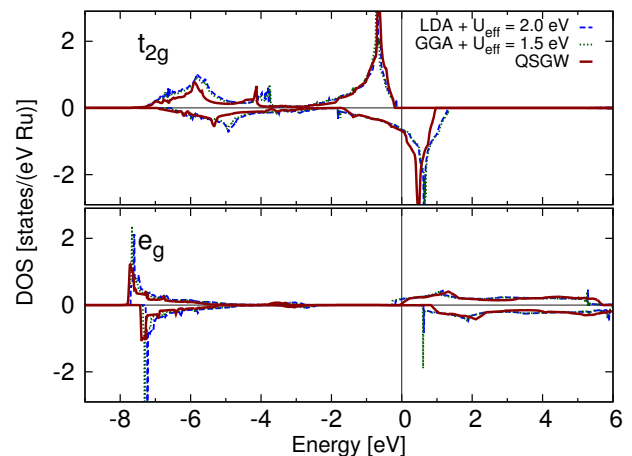


FIG. 9: The calculated Ru  $t_{2g}$  and  $e_g$  PDOS of cubic SRO113 by LDA+ $U$  ( $U_{\text{eff}} = 2.5$  eV) (blue dashed lines), GGA+ $U$  ( $U_{\text{eff}} = 2.0$  eV) (green dotted lines) and QSGW (red solid lines). The Fermi level is set to zero. The positive and negative DOS represent the up- and down-spin parts, respectively.

QSGW correlations but also the effect of orthorhombic distortion [4, 64, 90].

Together with the bandwidth reduction and the enhanced exchange splitting, the QSGW electronic structure becomes half-metallic with a gap in the majority spin state. Note that this QSGW band structure is quite similar with DFT+ $U$  result [15, 16] as shown in Fig. 9. The calculated magnetic moment of QSGW is  $\mu = 2.0\mu_B/\text{f.u.}$  which is significantly larger than the LDA value and comparable with the DFT+ $U$  results [15–17]. While we only considered the cubic structure, the effect of orthorhombic distortion is basically to enhance the on-site correlations as reported by the previous study [64, 90]. The experimental verification of the half-metallicity may not be easy because of the large magnetic fields required to overcome the magnetic anisotropy [55]. This possibility in SRO113 has been actively discussed based on DFT+ $U$  calculations [15, 16] and hybrid functional [55]. Therefore our QSGW result adds a new promising aspect toward this direction.

The detailed comparison with DFT+ $U$  result is given in Fig. 9. The optimized values of  $U_{\text{eff}}$  are favorably compared with a recent constrained RPA result of  $U_{\text{eff}} = 2.1$  eV although it is calculated from the orthorhombic structure of SRO113 [17]. As for the DMFT calculations, several different choices of  $U$  and  $J$  have been made as in the case of SRO214. In terms of  $U_{\text{eff}} = U - J$ , it ranges from 1.75 to 2.4 eV [59, 91, 92].

Several photoemission spectroscopy (PES) experiments report the LHB-like feature at  $\sim -2$  eV [60, 61, 64]. The PES spectrum of orthorhombic phase [64] are plotted along with the calculated DOS by LDA,

LDA+DMFT [91], and QSGW in Fig. 5(b). The LHB-like peak near  $-1.5$  eV is observed in the PES spectra, while not in LDA and QSGW. It has been argued that this LHB-like feature is not related to the magnetic fluctuations or the orthorhombic structural distortion [64]. LDA+DMFT calculation of orthorhombic SRO113 with  $U = 3.5$  and  $J = 1.75$  eV predicts the LHB at  $-3 - -1$  eV [91] (Fig. 5(b)). As in SRO214, LHB is the characteristic feature of DMFT distinctive from QSGW (also from DFT+ $U$ ) while some DMFT results do not seem to support this feature [59]. The absence of this state in QSGW and DFT+ $U$  (see  $t_{2g}$  states of Fig. 9) indicates that it is related to the dynamic aspects of Ru-4d correlation hybridized with O-2p as in the case of Zhang-Rice band in cuprates. Also, regarding the half-metallic band structure, DMFT calculations do not seem to give a consistent prediction [91, 93]. These issues that is likely related to the intrinsic parameter dependency require further investigations.

#### IV. SUMMARY

Using QSGW calculations, we re-investigated the electronic structure of SRO214 and SRO113. Without any *ad hoc* parameter or the ambiguity related to the double-counting and downfolding issues, some of the important features of electron correlations were reasonably well captured such as the bandwidth renormalization and the exchange splitting. In the case of SRO113, QSGW result is

in good agreement with DFT+ $U$  in a reasonable range of  $U$  and  $J$  parameter. While the QSGW shows the limitation in describing the detailed features such as the Ru-4d spectral weight transfer to LHB, it can be improved in combination with other techniques as reported in recent studies [87, 94, 95]. Our result sheds new light on the possibility and the limitation of the first-principles electronic structure calculations of the moderately correlated transition-metal oxides systems.

#### V. ACKNOWLEDGEMENTS

S.R., S.W.J., and M.J.H. were supported by Basic Science Research Program through the National Research Foundation of Korea (NRF) (2014R1A1A2057202; Ministry of Education) and by Samsung Advanced Institute of Technology (SAIT). The computing resource is supported by National Institute of Supercomputing and Networking / Korea Institute of Science and Technology Information with supercomputing resources including technical support (KSC-2013-C2-024) and by Computing System for Research in Kyushu University. T.K. was supported by the Advanced Low Carbon Technology Research and Development Program (ALCA), the High-efficiency Energy Conversion by Spinodal Nanodecomposition program of the Japan Science and Technology Agency (JST), and the JSPS Core-to-Core Program Advanced Research Networks ("Computational Nano-materials Design on Green Energy").

- 
- [1] Y. Maeno, H. Hashimoto, K. Yoshida, S. Nishizaki, T. Fujita, J. G. Bednorz, and F. Lichtenberg, *Nature (London)* **372**, 532 (1994); G. M. Luke, Y. Fudamoto, K. M. Kojima, M. I. Larkin, J. Merrin, B. Nachumi, Y. J. Uemura, Y. Maeno, Z. Q. Mao, Y. Mori, H. Nakamura, and M. Sigrist, *Nature (London)* **394**, 558 (1998); K. Ishida, H. Mukuda, Y. Kitaoka, K. Asayama, Z. Q. Mao, Y. Mori, and Y. Maeno, *Nature (London)* **396**, 658 (1998); T. M. Rice and M. Sigrist, *J. Phys.: Condens. Matter* **7**, L643 (1995); G. Baskaran, *Physica B* **224**, 490 (1996).
- [2] J. Mravlje, M. Aichhorn, T. Miyake, K. Haule, G. Kotliar, and A. Georges, *Phys. Rev. Lett.* **106**, 096401 (2011).
- [3] L. de' Medici, J. Mravlje, and A. Georges, *Phys. Rev. Lett.* **107**, 256401 (2011).
- [4] A. Georges, L. de' Medici, and J. Mravlje, *Annu. Rev. Condens. Matter Phys.* **4** 137 (2013).
- [5] S. B. Chung, S. Raghu, A. Kapitulnik, and S. A. Kivelson, *Phys. Rev. B* **86**, 064525 (2012).
- [6] Q. H. Wang, C. Platt, Y. Yang, C. Honerkamp, F. C. Zhang, W. Hanke, T. M. Rice and R. Thomale, *EPL* **104**, 17013 (2013).
- [7] J.-W. Huo and F.-C. Zhang, *Phys. Rev. B* **87**, 134501 (2013).
- [8] C. Rastovski, C. D. Dewhurst, W. J. Gannon, D. C. Peets, H. Takatsu, Y. Maeno, M. Ichioka, K. Machida, and M. R. Eskildsen, *Phys. Rev. Lett.* **111**, 087003 (2013).
- [9] T. Scaffidi, J. C. Romers, and S. H. Simon, *Phys. Rev. B* **89**, 220510(R) (2014).
- [10] A. Callaghan, C. W. Moeller, and R. Ward, *Inorg. Chem.* **5**, 1573 (1966).
- [11] J. M. Longo, P. M. Raccah, and J. B. Goodenough, *J. Appl. Phys.* **39**, 1327 (1968).
- [12] J. J. Neumeier, A. L. Cornelius, and J. S. Schilling, *Physica B* **198**, 324 (1994).
- [13] A. Kanbayasi, *J. Phys. Soc. Jpn.* **41**, 1876 (1976).
- [14] G. Cao, S. McCall, M. Shepard, J. E. Crow, and R. P. Guertin, *Phys. Rev. B* **56**, 321 (1997).
- [15] H.-T. Jeng, S.-H. Lin, and C.-S. Hsue, *Phys. Rev. Lett.* **97**, 067002 (2006).
- [16] P. Mahadevan, F. Aryasetiawan, A. Janotti, and T. Sasaki, *Phys. Rev. B* **80**, 035106 (2009).
- [17] J. M. Rondinelli, N. M. Caffrey, S. Sanvito, and N. A. Spaldin, *Phys. Rev. B* **78**, 155107 (2008).
- [18] K. S. Takahashi, A. Sawa, Y. Ishii, H. Akoh, M. Kawasaki, and Y. Tokura, *Phys. Rev. B* **67**, 094413 (2003).
- [19] F. Le Marrec, A. Demuer, D. Jaccard, J.-M. Triscone, M. K. Lee, and C. B. Eom, *Appl. Phys. Lett.* **80**, 2338 (2002).
- [20] H. N. Lee, H. M. Christen, M. F. Chisholm, C. M. Rouleau, and D. H. Lowndes, *Appl. Phys. Lett.* **84**, 4107 (2004).

- [21] C. H. Ahn, T. Tybell, L. Antognazza, K. Char, R. H. Hammond, M. R. Beasley, Ø. Fischer, and J.-M. Triscone, *Science* **276**, 1100 (1997).
- [22] K. S. Takahashi, M. Gabay, D. Jaccard, K. Shibuya, T. Ohnishi, M. Lippmaa, and J.-M. Triscone, *Nature (London)* **441**, 195 (2006).
- [23] C. H. Ahn, R. H. Hammond, T. H. Geballe, M. R. Beasley, J.-M. Triscone, M. Decroux, Ø. Fischer, L. Antognazza, and K. Char, *Appl. Phys. Lett.* **70**, 206 (1997).
- [24] T. Oguchi, *Phys. Rev. B* **51**, 1385 (1995).
- [25] D. J. Singh, *Phys. Rev. B* **52**, 1358 (1995).
- [26] I. Hase and Y. Nishihara, *J. Phys. Soc. Jpn.* **65**, 3957 (1996).
- [27] G. J. McMullan, M. P. Ray, and R. J. Needs, *Physica B* **223-224**, 529 (1996).
- [28] C. Noce and M. Cuoco, *Phys. Rev. B* **59**, 2659 (1999).
- [29] A. P. Mackenzie, S. Ikeda, Y. Maeno, T. Fujita, S. R. Julian, G. G. Lonzarich, *J. Phys. Soc. Jpn.* **67**, 385 (1998).
- [30] A. P. Mackenzie, S. R. Julian, A. J. Diver, G. J. McMullan, M. P. Ray, G. G. Lonzarich, Y. Maeno, S. Nishizaki, and T. Fujita, *Phys. Rev. Lett.* **76**, 3786 (1996).
- [31] A. V. Puchkov, Z.-X. Shen, T. Kimura, and Y. Tokura, *Phys. Rev. B* **58**, R13322(R) (1998).
- [32] C. Bergemann, A. P. Mackenzie, S. R. Julian, D. Forsythe, and E. Ohmichi, *Adv. Phys.* **52**, 639 (2003).
- [33] H. Iwasawa, Y. Aiura, T. Saitoh, I. Hase, S. I. Ikeda, Y. Yoshida, H. Bando, M. Higashiguchi, Y. Miura, X. Y. Cui, K. Shimada, H. Namatame, and M. Taniguchi, *Phys. Rev. B* **72**, 104515 (2005).
- [34] C. Bergemann, S. R. Julian, A. P. Mackenzie, S. Nishizaki, and Y. Maeno, *Phys. Rev. Lett.* **84**, 2662 (2000).
- [35] D. H. Lu, M. Schmidt, T. R. Cummins, S. Schuppler, F. Lichtenberg, and J. G. Bednorz, *Phys. Rev. Lett.* **76**, 4845 (1996).
- [36] T. Yokoya, A. Chainani, T. Takahashi, H. Ding, J. C. Campuzano, H. Katayama-Yoshida, M. Kasai, and Y. Tokura, *Phys. Rev. B* **54**, 13311 (1996).
- [37] A. Damascelli, D. H. Lu, K. M. Shen, N. P. Armitage, F. Ronning, D. L. Feng, C. Kim, Z.-X. Shen, T. Kimura, Y. Tokura, Z. Q. Mao, and Y. Maeno, *Phys. Rev. Lett.* **85**, 5194 (2000).
- [38] R. Matzdorf, Z. Fang, Ismail, Jiandi Zhang, T. Kimura, Y. Tokura, K. Terakura, and E. W. Plummer, *Science* **289**, 746 (2000).
- [39] K. M. Shen, A. Damascelli, D. H. Lu, N. P. Armitage, F. Ronning, D. L. Feng, C. Kim, Z.-X. Shen, D. J. Singh, I. I. Mazin, S. Nakatsuji, Z. Q. Mao, Y. Maeno, T. Kimura, and Y. Tokura, *Phys. Rev. B* **64**, 180502(R) (2001).
- [40] T. Yokoya, A. Chainani, T. Takahashi, H. Katayama-Yoshida, M. Kasai, Y. Tokura, N. Shanthi, and D. D. Sarma, *Phys. Rev. B* **53**, 8151 (1996).
- [41] I. H. Inoue, Y. Aiura, Y. Nishihara, Y. Haruyama, S. Nishizaki, Y. Maeno, Y. Fujita, J. G. Bednorz, and F. Lichtenberg, *Physica B* **223-224**, 516 (1996).
- [42] I. H. Inoue, A. Kimura, A. Harasawa, A. Kakizaki, Y. Aiura, S. Ikeda, and Y. Maeno, *J. Phys. Chem. Solids* **59**, 2205 (1998).
- [43] T. T. Tran, T. Mizokawa, S. Nakatsuji, H. Fukazawa, and Y. Maeno, *Phys. Rev. B* **70**, 153106 (2004).
- [44] A. Pérez-Navarro, J. Costa-Quintana, and F. López-Aguilar, *Phys. Rev. B* **61**, 10125 (2000).
- [45] Z. V. Pchelkina, I. A. Nekrasov, Th. Pruschke, A. Sekiyama, S. Suga, V. I. Anisimov, and D. Vollhardt, *Phys. Rev. B* **75**, 035122 (2007).
- [46] A. Liebsch and A. Lichtenstein, *Phys. Rev. Lett.* **84**, 1591 (2000).
- [47] D. J. Singh, *Phys. Rev. B* **77**, 046101 (2008).
- [48] Z. V. Pchelkina, I. A. Nekrasov, Th. Pruschke, S. Suga, V. I. Anisimov, and D. Vollhardt, *Phys. Rev. B* **77**, 046102 (2008).
- [49] V. I. Anisimov, F. Aryasetiawan, and A. I. Lichtenstein, *J. Phys.: Condens. Matter* **9**, 767 (1997); G. Kotliar, S. Y. Savrasov, K. Haule, V. S. Oudovenko, O. Parcollet, and C. A. Marianetti, *Rev. Mod. Phys.* **78**, 865 (2006).
- [50] P. B. Allen, H. Berger, O. Chauvet, L. Forro, T. Jarlborg, A. Junod, B. Revaz, and G. Santi, *Phys. Rev. B* **53**, 4393 (1996).
- [51] G. Santi and T. Jarlborg, *J. Phys.: Condens. Matter* **9**, 9563 (1997).
- [52] I. I. Mazin and D. J. Singh, *Phys. Rev. B* **56**, 2556 (1997).
- [53] Y. J. Chang, C. H. Kim, S.-H. Phark, Y. S. Kim, J. Yu, and T. W. Noh, *Phys. Rev. Lett.* **103**, 057201 (2009).
- [54] J. Xia, W. Siemons, G. Koster, M. R. Beasley, and A. Kapitulnik, *Phys. Rev. B* **79**, 140407(R) (2009).
- [55] M. Verissimo-Alves, P. García-Fernández, D. I. Bilc, P. Ghosez, and J. Junquera, *Phys. Rev. Lett.* **108**, 107003 (2012).
- [56] K. Gupta, B. Mandal, and P. Mahadevan, *Phys. Rev. B* **90**, 125109 (2014).
- [57] L. Si, Z. Zhong, J. M. Tomczak, and K. Held, *Phys. Rev. B* **92**, 041108(R) (2015).
- [58] P. Werner, E. Gull, M. Troyer, and A. J. Millis, *Phys. Rev. Lett.* **101**, 166405 (2008).
- [59] H. T. Dang, J. Mravlje, A. Georges, and A. J. Millis, *Phys. Rev. B* **91**, 195149 (2015).
- [60] K. Fujioka, J. Okamoto, T. Mizokawa, A. Fujimori, I. Hase, M. Abbate, H. J. Lin, C. T. Chen, Y. Takeda, and M. Takano, *Phys. Rev. B* **56**, 6380 (1997).
- [61] J. Okamoto, T. Mizokawa, A. Fujimori, I. Hase, M. Nohara, H. Takagi, Y. Takeda, M. Takano, *Phys. Rev. B* **60**, 2281 (1999).
- [62] H.-D. Kim, H.-J. Noh, K. H. Kim, and S.-J. Oh, *Phys. Rev. Lett.* **93**, 126404 (2004); J. Park, S.-J. Oh, J.-H. Park, D. M. Kim, and C.-B. Eom, *Phys. Rev. B* **69**, 085108 (2004); W. Siemons, G. Koster, A. Vailionis, H. Yamamoto, D. H. A. Blank, and M. R. Beasley, *Phys. Rev. B* **76**, 075126 (2007); E. B. Guedes, M. Abbate, K. Ishigami, A. Fujimori, K. Yoshimatsu, H. Kumigashira, M. Oshima, F. C. Vicentin, P. T. Fonseca, and R. J. O. Mossaneck, *Phys. Rev. B* **86**, 235127 (2012).
- [63] K. Maiti and R. S. Singh, *Phys. Rev. B* **71**, 161102(R) (2005).
- [64] M. Takizawa, D. Toyota, H. Wadati, A. Chikamatsu, H. Kumigashira, A. Fujimori, M. Oshima, Z. Fang, M. Lippmaa, M. Kawasaki, and H. Koinuma, *Phys. Rev. B* **72**, 060404(R) (2005).
- [65] S. V. Faleev, M. van Schilfhaarde, and T. Kotani, *Phys. Rev. Lett.* **93**, 126406 (2004).
- [66] M. van Schilfhaarde, T. Kotani, and S. Faleev, *Phys. Rev. Lett.* **96**, 226402 (2006).
- [67] T. Kotani, M. van Schilfhaarde, and S. V. Faleev, *Phys. Rev. B* **76**, 165106 (2007).
- [68] J. Klimeš, M. Kaltak, and G. Kresse, *Phys. Rev. B* **90**, 075125 (2014).
- [69] F. Bruneval, *J. Chem. Phys.* **136**, 194107 (2012).
- [70] R. Shaltaf, G. -M. Rignanese, X. Gonze, F. Giustino, and A. Pasquarello, *Phys. Rev. Lett.* **100**, 186401 (2008).



- [71] W. R. L. Lambrecht, *Physica Status Solidi B* **248**, 1547 (2011).
- [72] S. W. Jang, T. Kotani, H. Kino, K. Kuroki, and M. J. Han, *Sci. Rep.* **5**, 12505 (2015).
- [73] T. Kotani and M. van Schilfgaarde, *J. Phys.: Condens. Matter* **20**, 295214 (2008).
- [74] M. J. Han, H. Kino, and T. Kotani, *Phys. Rev. B* **90**, 035127 (2014).
- [75] A. N. Chantis, M. van Schilfgaarde, and T. Kotani, *Phys. Rev. B* **76**, 165126 (2007).
- [76] The electronic structure simulation package, “ecalj” implemented by T. Kotani. <https://github.com/tkotani/ecalj>; LMTO electronic structure simulation package, “LM Suite”. <http://www.lmsuite.org>.
- [77] T. Kotani, *J. Phys. Soc. Jpn.* **83**, 094711 (2014); T. Kotani and M. van Schilfgaarde, *Phys. Rev. B* **81**, 125117 (2010); T. Kotani and H. Kino, *J. Phys. Soc. Jpn.* **82**, 124714 (2013); T. Kotani, H. Kino, and H. Akai, *J. Phys. Soc. Jpn.* **84**, 034702 (2015).
- [78] B. C. Chakoumakos, S. E. Nagler, S. T. Misture, H. M. Christen, *Physica B* **241-243**, 358 (1998).
- [79] It is found that the inclusion of M-point ( $\pi,0,0$ ) is important due to the existence of van Hove singularity. As a result, the result of  $7\times 7\times 7$   $\mathbf{k}$  points shows the unusually large deviation from the  $6\times 6\times 6$  result. Due to the large computation cost, we could not further increase the number of  $\mathbf{k}$  points.
- [80] T. Ozaki, *Phys. Rev. B* **67**, 155108 (2003).
- [81] J. P. Perdew and A. Zunger, *Phys. Rev. B* **23**, 5048 (1981).
- [82] J. P. Perdew, K. Burke, and M. Ernzerhof, *Phys. Rev. Lett.* **77**, 3865 (1996).
- [83] S. L. Dudarev, G. A. Botton, S. Y. Savrasov, C. J. Humphreys, and A. P. Sutton, *Phys. Rev. B* **57**, 1505 (1998).
- [84] M. J. Han, T. Ozaki, and J. Yu, *Phys. Rev. B* **73**, 045110 (2006).
- [85] M. W. Haverkort, I. S. Elfimov, L. H. Tjeng, G. A. Sawatzky, and A. Damascelli, *Phys. Rev. Lett.* **101**, 026406 (2008).
- [86] There is no significant difference between DOS and  $A(\omega)$  obtained by QSGW (see Fig. 2(e)). Therefore in the below, our discussion will mainly be based on DOS.
- [87] J. M. Tomczak, M. Casula, T. Miyake, and S. Biermann, *Phys. Rev. B* **90**, 165138 (2014).
- [88] H. Iwasawa, Y. Yoshida, I. Hase, S. Koikegami, H. Hayashi, J. Jiang, K. Shimada, H. Namatame, M. Taniguchi, and Y. Aiura, *Phys. Rev. Lett.* **105**, 226406 (2010).
- [89] We estimated  $Z_{\text{QSGW}}^{-1}$  at  $\Gamma$  point.
- [90] E. Pavarini, S. Biermann, A. Poteryaev, A. I. Lichtenstein, A. Georges, and O. K. Andersen, *Phys. Rev. Lett.* **92**, 176403 (2004).
- [91] E. Jakobi, S. Kanungo, S. Sarkar, S. Schmitt, and T. Saha-Dasgupta, *Phys. Rev. B* **83**, 041103(R) (2011).
- [92] O. Grånäs, I. Di Marco, O. Eriksson, L. Nordström, and C. Etz, *Phys. Rev. B* **90**, 165130 (2014).
- [93] M. Kim and B. I. Min, *Phys. Rev. B* **91**, 205116 (2015).
- [94] J. M. Tomczak, M. van Schilfgaarde, and G. Kotliar, *Phys. Rev. Lett.* **109**, 237010 (2012).
- [95] S. Choi, A. Kutepov, K. Haule, M. van Schilfgaarde, and G. Kotliar, arXiv:1504.07569.